Journal of Groundwater Science and Engineering
ISSN 2305-7068
Indexed by ESCI CABI CSA
Scopus GeoRef AJ CNKI

Genetic model and exploration target area of geothermal resources in Hongtang Area, Xiamen, China

Chun-lei Liu, Chen-ming Lu, Ya-song Li, Qi-chen Hao, Sheng-wei Cao

Citation:
Liu CL, Lu CM, Li YS, *et al*. 2022. Genetic model and exploration target area of geothermal resources in Hongtang Area, Xiamen, China. Journal of Groundwater Science and Engineering, 10(2): 128-137.

View online: https://doi.org/10.19637/j.cnki.2305-7068.2022.02.003

Articles you may be interested in

Geothermal resources formation conditions and preferred target areas in a certain county of Western Sichuan,China
Journal of Groundwater Science and Engineering. 2019, 7(1): 61-69

Study on multiple induced polarization parameters in groundwater exploration in Bashang poverty alleviation area of Heibei Province, China
Journal of Groundwater Science and Engineering. 2020, 8(3): 274-280 https://doi.org/10.19637/j.cnki.2305-7068.2020.03.007

Experimental simulation and dynamic model analysis of Cadmium (Cd) release in soil affected by rainfall leaching in a coal-mining area
Journal of Groundwater Science and Engineering. 2021, 9(1): 65-72 https://doi.org/10.19637/j.cnki.2305-7068.2021.01.006

Causes of geothermal fields and characteristics of ground temperature fields in China
Journal of Groundwater Science and Engineering. 2019, 7(1): 15-28

Application of CSAMT in hydrogeology exploration in Shandong Province–An example from geothermal exploration in Changdao County (south four islands)
Journal of Groundwater Science and Engineering. 2018, 6(1): 58-64 https://doi.org/10.19637/j.cnki.2305-7068.2018.01.007

Pollution pattern of underground river in karst area of the Southwest China
Journal of Groundwater Science and Engineering. 2018, 6(2): 71-83

Journal of Groundwater Science and Engineering 10(2022) 128–137

Journal homepage: http://gwse.iheg.org.cn

Genetic model and exploration target area of geothermal resources in Hongtang Area, Xiamen, China

Chun-lei Liu[1,2], Chen-ming Lu[1*], Ya-song Li[1], Qi-chen Hao[1], Sheng-wei Cao[1]

[1] *Institute of Hydrogeology and Environmental Geology*, *Chinese Academy of Geological Sciences*, *Shijiazhuang* 050061, *China*.
[2] *Fujian Provincial Key Laboratory of Water Cycling and Eco-Geological Processes*, *Xiamen* 361000, *Fujian Province*, *China*.

Abstract: The geothermal resources in Fujian Province are mainly hydrothermal resources of medium-low temperature. To better understand the whole process and conditions of heat control in the middle and deep crust, this study focuses on the analysis of heat accumulation model in Hongtang Area of Xiamen, and the main conditions of the model such as faults and sags are explored and interpreted in detail by using gravity and wide-field electromagnetic methods. 4 main faults (F33, F2, F12 and HT-F1) and 10 secondary faults (HT-F2, HT-F3, HT-F4, HT-F5, HT-F6, HT-F7, HT-F8, HT-F9, HT-F10 and HT-F11) were inferred, and the distribution range of sags was delineated. The convective geothermal system is composed of four components: Heat source, geothermal reservoir, heat-conductive fault and heat retaining cover, which form a quaternary heat accumulation model. According to the model, the intersection of the main faults F12, HT-F1 and F33 can be delineated as the primary target area of geothermal exploration, while the intersection of the secondary faults (F12 and HT-F6; F12 and HT-F2; HT-F9, HT-F10 and F12; F12 and HT-F11; F33 and HT-F3; HT-F8 and HT-F3; HT-F2, HT-F10 and HT-F1) can be delineated as the secondary target area. Borehole DR01, which is located in the primary target area, shows that the water temperature increases from fast to slow in the depth range of 0–500 m, and stays at 36℃ below 500 m. The reliability of the heat accumulation model and the target area was tested via geothermal boreholes, which is of great significance to the exploitation and utilization of geothermal resources in Hongtang Area of Xiamen.

Keywords: Geotherm; Gravity method; Wide-field electromagnetic method; Target area of geothermal exploration; Heat accumulation model; Hongtang Area

Received: 09 Apr 2021/ Accepted: 03 Apr 2022

2305-7068/© 2022 Journal of Groundwater Science and Engineering Editorial Office

Introduction

As a province with many hot springs in China, Fujian ranks only behind Yunnan, Tibet, Sichuan and Guangdong (Liao, 2012; Gao et al. 2018). According to Zhuang (2015), there are 215 hot springs in the province, including 22 boreholes and 193 natural ones. Among them, 10 natural springs and 8 drilled holes have temperature exceeding 80℃(Zhuang, 2015). The distribution of hot springs and geothermal boreholes are strongly controlled by fault zones (Zhang et al. 2019; Wang et al. 2020). The NE trending faults are compression-shear and the NW trending faults are tension-shear, the latter of which often become the main channel for geothermal fluid discharge (Wan et al. 1987, 1988) (Fig. 1). From the perspective of tectonics, Fujian is located at the junction of Eurasian plate, Pacific plate and Philippine plate, and has experienced collisions and subductions, which are related to the strong tectono-magmatic activity during Meso-Cenozoic, as part of the Pacific Rim magmatic belt (Zhou et al. 2000; Chen et al. 2002; Zheng et al. 2013; Lin et al. 2015; Teng et al. 2017). The NE and NW-trending faults are strictly controlled by this tectonic settings (Wan et al. 1987). The crustal heat source of hot springs in Fujian province is rich in radioactive elements U, Th, K and so on, which may be associated with granite (Lin et al. 2016). In addition to crustal heat source, mantle-derived magma is also an important heat source of hot

*Corresponding author: Chen-ming Lu, *E-mail address*: luchenming@mail.cgs.gov.cn

DOI: 10.19637/j.cnki.2305-7068.2022.02.003

Liu CL, Lu CM, Li YS, et al. 2022. Genetic model and exploration target area of geothermal resources in Hongtang Area, Xiamen, China. Journal of Groundwater Science and Engineering, 10(2): 128-137.

springs (Wan et al. 1988; Xiong et al. 1991; Liao, 2012; Lin et al. 2019; Wu et al. 2019). Under ideal heat generation conditions of both crust and mantle, the terrestrial heat flow in granite area along the southeast coast can exceed 100 μW/m^2 (Lin et al. 2016). Therefore, Fujian province has good geothermal conditions and abundant geothermal resources (Wan et al. 1988).

In addition to geological conditions, the survey of regional geological structure is also very important for the development of geothermal resources in Fujian Province. Gravity and wide-field electromagnetic methods have been extensively used as important surveying methods (Goldstein et al. 1975; Ward, 1980) Among them, Bougher gravity anomaly is the comprehensive reflection of abnormal density mass at different depths in the gravity field (Ma et al. 2006). Gravity data not only reflects the distribution of geological mass and the characteristics of deep structures from the plane, but also contains important information of the field source with a greater spatial scale (Hao et al. 1997; Shao, 2013). Therefore, effective gravity data processing methods can help to understand the characteristics of gravity anomalies and identify regional structures successfully (Fang et al. 2002). Wide-field electromagnetic method inherits the advantages of controllable field source of CSAMT, and overcomes the disadvantages of magnetotelluric method such as random field source and weak signal (He, 2020). This method achieves large-area, great depth, high-precision, high-efficiency and multi-parameter detection of geological structures (He, 2019). In the process of structural interpretation, gravity method can help to detect the distribution of structures in the area, which has the advantage of transverse "plane", while wide-field electromagnetic method can interpret the properties and morphology of structures, which has the advantage of longitudinal "morphology". These two methods can be used together to interpret structures in a stereoscopic way.

The study area is located in Hongtang Village, Xiamen city. A commercial hot spring pool was developed with a water temperature of 61℃ previously, but the scale of the development and the investigation are far from meeting the local demand for geothermal resources. As an important geothermal exploration area in Fujian Province, the geological structures in the area are the key factors for further development and utilization of geothermal resources. However, most of the study area is covered by quaternary deposits, which results in the lack of research on the geological structure in the area. Therefore, gravity and wide-field electromagnetic methods were used to survey and interpret the faults and sags in the area in detail. Based on the result, the exploration target area is delineated and the reliability of the research results is validated by geothermal drilling.

1 Geological characteristics

The study area is located in the alluvial-pluvial plain near the estuary of Xixi in Xiamen City, which is a volcanic rock area along the southeast coast of China. Most of the area is covered by alluvial-pluvial deposits, eluvium-slope deposits and marine deposits, with very limited bedrock outcropped (Fig. 1). The alluvial-pluvial deposits are mainly composed of light grayish-yellow medium-coarse sand, conglomeratic sand and pebble, interbedded with sandy clay. The eluvium-slope deposits mainly consist of red sandy clay, clayey sand, breccia-containing clay sand and gravel. The marine deposits are basically silt and sandy silt. Quaternary sediments and weathering crust form the heat-retaining cap, which is more than 100 meters thick. The bedrocks are dominated by granodiorite and monzogranite, acting as the geothermal reservoir in the study area.

2 Exploration methods

In the gravity survey, static, dynamic and conformance tests were performed on the CG-5 gravimeter to meet the calibration accuracy required by the specification for gravitational field operation. Before the gravity survey, the instrument is calibrated in the order of base point-auxiliary base point-base point until operation is normal. Three numbers are read at the reference point and two at the measurement point. The average value is used for calculation. The survey lines are arranged in regular grid. When the regular gridline encounters obstacles, it can be deployed in a semi-free grid with the size of 250 m×50 m.

The instrument system developed by Hunan Jishan High-tech Co., Ltd was used in the wide-field electromagnetic survey. The system used the power source supplied by a pair of grounding electrodes as the field source to measure the horizontal component of the electric field which is parallel to the direction of the grounding electrodes. To ensure the reliability of the data, the consistency test for 12 channels of 2 instruments was carried out in the laboratory. The spacing of points in this work is 100 m. In field construction, 7 frequency

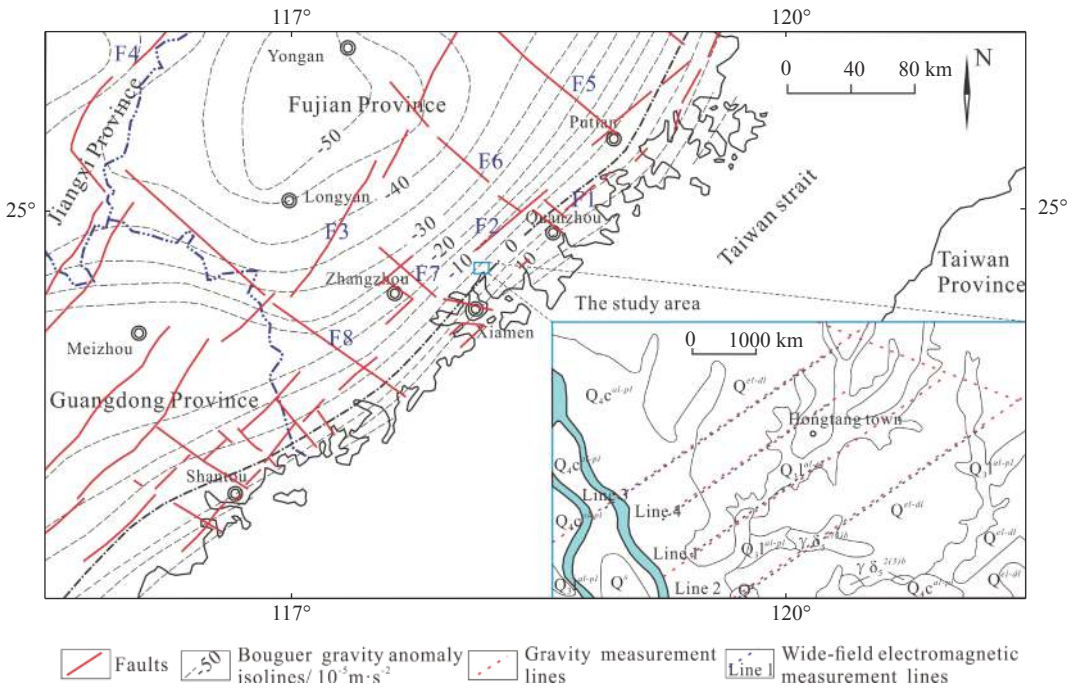

Fig. 1 Bouguer gravity isolines in the southeast coastal area and location map of the study area (modified from Chen et al. (1992) and Li et al. (2019))

Notes: Q^{s}—Artificial accumulation; $Q_4c^{al\text{-}pl}$—Alluvial-pluvial deposits (Changle Formation); $Q_3l^{al\text{-}pl}$—Alluvial-pluvial deposits (Longhai Formation); $Q^{el\text{-}dl}$—Eluvium-slope deposits; $\gamma\delta_5^{2(3)b}$—Granodiorite; F1—Changle-Shaoan fault; F2—Nanxi-Lufeng fault; F3—Zhenghe-Dapu fault; F4—Shaowu-Heyuan fault; F5—Shaxian-Nanridao fault; F6—Yongan-Jinjiang fault; F7—Jiulongjiang fault; F8—Shanghang-Yunxiao fault.

waves (3, 4, 5, 6, 7, 8, 9, 10, 11) of pseudo-random signals were used for power supply. The frequency range is 8 192 Hz to 0.015 625 Hz for a total of 62 frequency points.

3 Gravity and wide-field electromagnetic characteristics

Hongtang Area of Xiamen is located in a gravity anomaly gradient belt, where the outliers are mainly negative. The anomaly variation is increasing from west to east with gravity values ranging from -33.5×10^{-5} m/s^2 to -22.5×10^{-5} m/s^2. Bouguer gravity value has a wide range with the higher limit of 11×10^{-5} m/s^2, and an average of 1.5×10^{-5} m/s^2 per kilometer (Fig. 2C). Generally, the gradient belt has a NNE to SSW trend, whereas in the middle zone it is suddenly bent and presents the shape of inverted "Z" (Fig. 2C). According to the upward comparison map of Bouguer gravity anomaly (50 m, 100 m, 200 m), the outliers decay very slowly and the range of the anomaly changes little (Fig. 2). The 200 m map shows the sparse isolines, gentle gradient zone and increasing gravity value (Fig. 2A). The changes from Fig. 2C to Fig. 2A indicate that the "high frequency" anomalies caused by shallow field source mass decay rapidly with the increase of height and are locally tapered out, while the "low frequency" anomalies caused by large and deep field source mass decay slowly in a wide range. The trendline of relatively low anomaly indicated by the red line in the figure always exists with the increase of the upward elevation, following the same direction from west to east.

The background field can be calculated based on Bouguer gravity anomaly data. The average deviation of the fifth-order trend surface is the smallest, which may be the ideal background field. The red and blue areas represent the high and low residual gravity anomaly zones respectively, and the yellow dotted line indicates the zero-value line. The residual gravity anomaly ranges from -0.9×10^{-5} m/s^2 to 0.8×10^{-5} m/s^2 and the spacing of the isolines is 0.1×10^{-5} m/s^2 (Fig. 3D). The low residual gravity anomaly zones show a zonal distribution of NW- and NE-trending, and some are EW-trending. We delineated 29 zones in the residual gravity anomaly map, including 17 high residual gravity anomaly zones and 12 low residual gravity anomaly zones. Each zone was numbered in the order from south to north, west to east and small to large.

Based on the statistics of aeromagnetic anomaly in the study area, the electrical characteristics of various rock types are summarized as follows: The

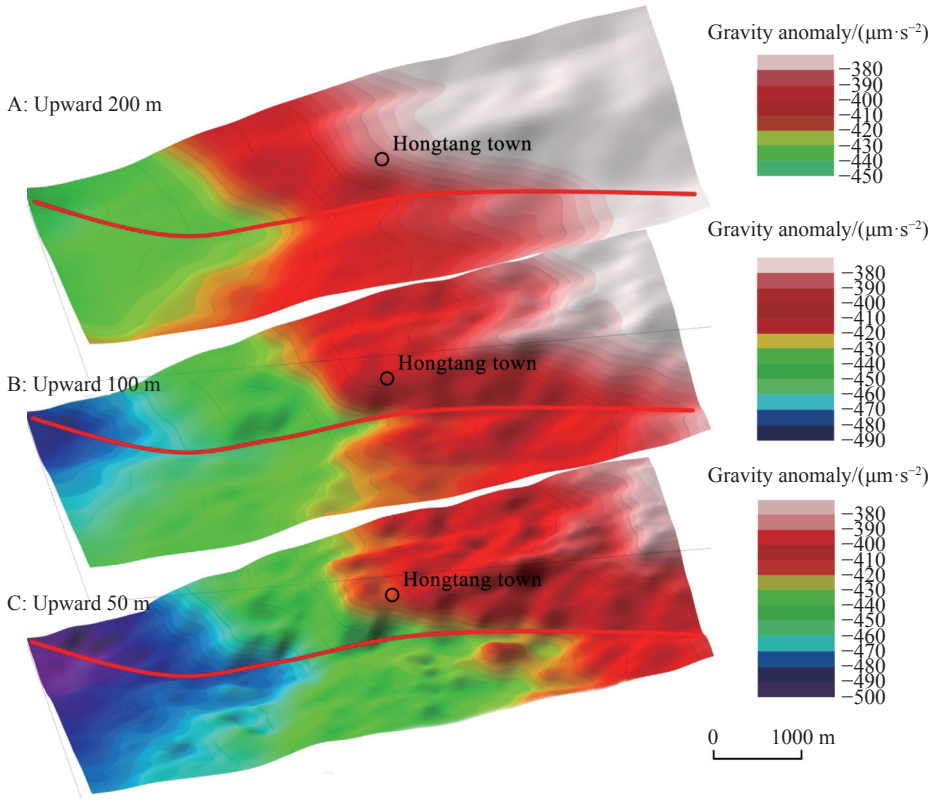

Fig. 2 The upward comparison map of Bouguer gravity anomaly in Hongtang Area of Xiamen (50 m, 100 m, 200 m)

Notes: A: Upward 200 m; B: Upward 100 m; C: Upward 50 m.

resistivity of monzogranite varies from 4 500 Ω•m to 5 867 Ω•m, with a common value of 5 158 Ω•m; The resistivity of the granodiorite varies from 1 959 Ω•m to 3 990 Ω•m, with a common value of 2 454 Ω•m. It is found that the Quaternary and the fault fracture zone in the area have low resistivity. Granitoids is characterized by high resistivity, but the resistivity of intrusive rocks in early Yanshan is lower than that of the late intrusive rocks.

4 Interpretation methods of gravity and wide-field electromagnetism

According to Bouguer gravity anomaly map and the extended maps, the basic interpretation methods of fault are as follows: 1) Gravity anomaly gradient belt. Linear gradient is the zone, where the material of crust or upper mantle changes dramatically along the horizontal direction. It is the dividing line of the rise and fall in different crustal blocks. In fact, gradient belt with long duration are often the reflection of regional faults, which can be divided into two types: Linear gradient belt and linear arrangement of gradient belt; 2) Linear transition belt of anomaly. The boundary between high and low gravity anomaly zones is also a reflection of faults; 3) Long and narrow anomaly belt or linear anomaly belt, where the long axis is much longer than the short axis, tends to be a reflection of faults, even with a small gradient; 4) Isoline of regular distortion. Local disturbance on the background of isoline trend, coaxial distortion of the flat contour of isoline, and sharp convergence of isoline at a certain position can also be interpreted as faults; 5) A boundary on both sides of which the anomaly characteristics are obviously different. It mainly reflects the great difference in the structural characteristics of the two sides, which is often a large scale regional fault; 6) Linear truncations or staggered parts of multiple anomalies arranged side by side are often related to faults; 7) The trend line in the upward comparison map of Bouguer gravity anomaly could also be interpreted as fault; 8) The zero line of the vertical second derivative may be a fault.

The basic interpretation methods of sag are as follows: 1) Bouguer gravity anomaly map. The low gravity zones surrounded by the high gravity zones may be sag areas; 2) Residual gravity anomaly map. The overlap of low residual gravity anomaly and low Bouguer gravity anomaly should be sag areas; 3) Upward comparison map of Bouguer gravity anomaly. The place where Bouguer gravity anomaly disappears in the upward process may be

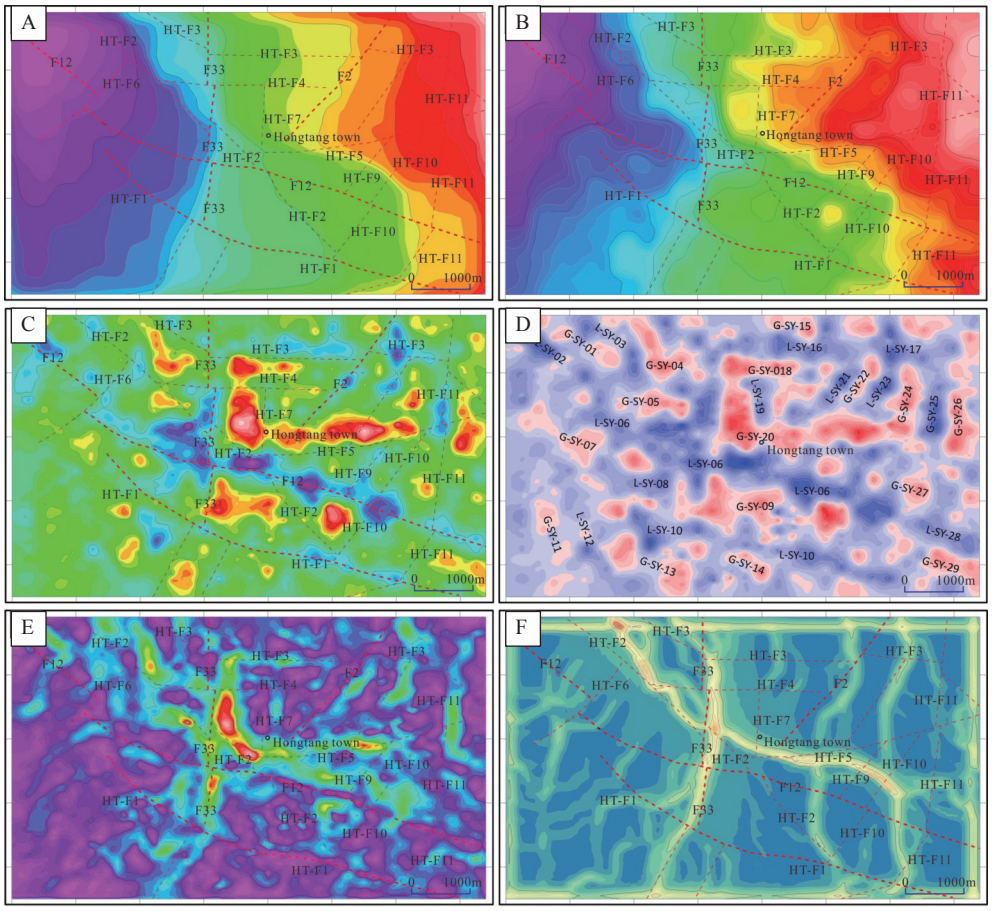

Fig. 3 Extended map of Bouguer gravity anomaly in Hongtang Area of Xiamen

Notes: A: Modular map of horizontal gradient (upward 50m); B: Modular map of horizontal gradient (upward 500m); C: Linear enhancement map (upward 50m); D: Linear enhancement map (upward 500m); E: Vertical second derivative map; F: Residual gravity anomaly map

sag areas; 4) Gravity anomaly gradient belt. The sparse areas in the Gravity anomaly gradient belt may be secondary sag areas.

The basic interpretation methods of wide-field electromagnetism are as follows: 1) By analyzing the electrical properties of rocks in the area using statistical method, it provides a reliable basis for the establishment of geological geophysical model, forward and inverse calculation and data interpretation; 2) The fault is inferred based on the gradient map of the inversion profile. The inferred results are calibrated and corrected by 1D and 2D continuum inversion; 3) Sequence division is determined by electrical properties of rocks in the area and regional geological data. Based on the characteristics of wide-field electromagnetism and gravity, the geological interpretation can be reasonably carried out.

5 Discussion

5.1 The interpretation of faults and sags

According to the structural map interpreted from the gravity data, three groups of faults in the direction of NE, NW and nearly SN are identified in Hongtang Area of Xiamen. The main faults are F33, F2, F12 and HT-F1, and the secondary faults are HT-F2, HT-F3, HT-F4, HT-F5, HT-F6, HT-F7, HT-F8, HT-F9, HT-F10 and HT-F11. In Bouguer gravity anomaly map, the fault F12 shows a sudden change of the NNE-trending gravity anomaly gradient belt and parallel distortion to the isoline in the direction of F12 (Fig. 2C). The isolines in the upward linear enhancement maps (50 m, 500 m) have the same characteristics (Fig. 3A, Fig. 3B). In upward comparison map of Bouguer gravity anomaly (50 m, 100 m, 200 m), the trend of relatively low anomaly direction along the fault F12 always exists with the increase of upward height (Fig. 2). In the vertical second derivative map, the position of fault F12 shows a beaded distribution of low anomaly zones (Fig. 3C). In the wide-field electromagnetic profile, the resistivity at the location of fault F12 is shown as a three-layer structure of low-high-low values from top to bottom (Fig. 4). The high resistance zone may be truncated and extended by the low resistance zone

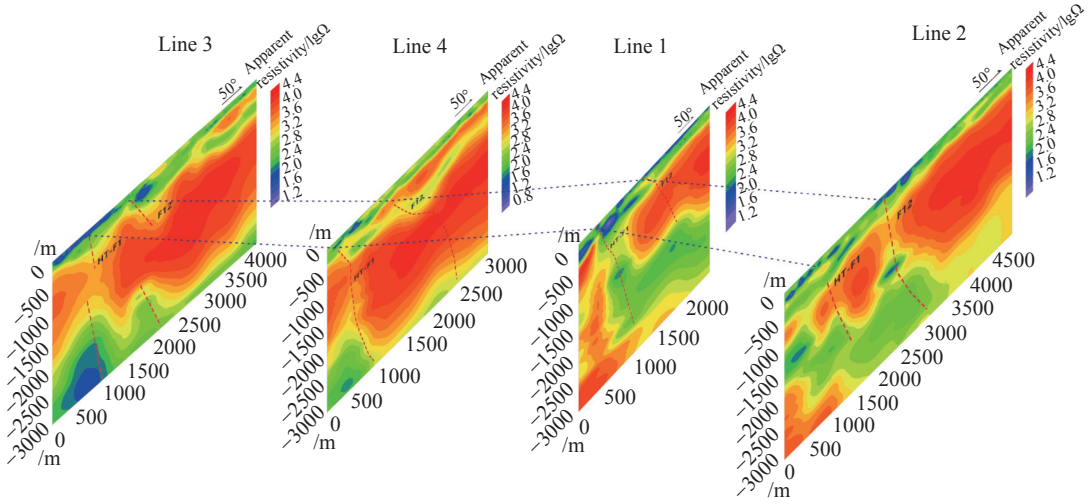

Fig. 4 Wide-area electromagnetic profile in Hongtang Area of Xiamen

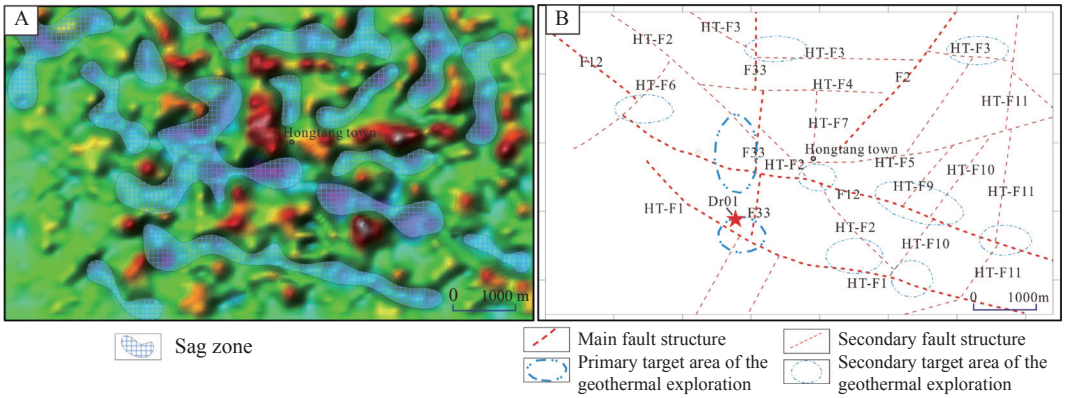

Fig. 5 Inferred result maps in Hongtang Area of Xiamen

Notes: A: Locations of the delineated sags; B: Locations of the inferred faults and target areas of geothermal exploration

(Line 1, Line 2, Line 3, Line 4). The reason for the phenomenon should be that the fault cuts the high-resistance granite, and reduces its resistivity. According to the wide-area electromagnetic characteristics, it is speculated that the fault F12 is a NW normal fault with a dip angle of about 50°–70°. The fault HT-F1 is shown in Fig. 2C, Fig. 3A, Fig. 3B as parallel distortion to the isoline in SE direction, which can also be identified in Fig. 3C. In the wide-field electromagnetic profile, the fault HT-F1 mainly shows that the high resistance zone is truncated and extended by the low resistance zone (Fig. 4). It is speculated that HT-F1 is a NW normal fault with a dip angle of about 60°–80°. The fault F33 shows sharp convergence of isolines in Fig. 2C, Fig. 3E and Fig. 3F, and the zonal distribution of anomaly zones in Fig. 3C. The fault F2 is shown as a low anomaly zones with a beaded distribution in Fig. 2C, and can also be identified in Fig. 3C. The secondary faults in the study area are mainly inferred from the upward linear enhancement maps and the vertical second derivative map, which mainly show as parallel distortion and sharp convergence of isolines and low anomaly zones with zonal distribution. Some secondary faults also have the characteristics of parallel distortion and sharp convergence of isolines in Bouguer gravity anomaly map.

In areas with uniform bedrock types, the phenomenon that the high gravity anomaly zones and the low gravity anomaly zones are surrounded by each other in Bouguer gravity anomaly map is usually caused by alternative sag and uplift. In order to identify the specific locations of sag and uplift, we select the appropriate background field to calculate the residual gravity anomaly. After eliminating the interference of background field, the scale of sag and uplift can be delineated by residual gravity anomaly (Fig. 3D). In the vertical second derivative map, the relative depth and scale of sags can also be well presented (Fig. 3C). In the wide-field electromagnetic profile, the low resis-

tivity zone on the surface is mainly related to the loose sediments of the Quaternary and the deep weathered layer caused by faults. Its relative thickness also indicates the scale and depth of the sag (Fig. 4). In general, "large" sags are distributed at the intersections of fault F33 with fault F22 and HT-F1, and relatively small sags are also developed in other areas (Fig. 5).

5.2 Analysis of heat accumulation model

At present, the geothermal resources in Fujian Province are mainly hydrothermal resources with medium-low temperature (<150℃) (Wan et al. 1988). From the perspective of thermal contribution, Pang (1987) found that mantle-derived heat in Zhangzhou Area accounts for about 60%, while the radioactive element decay accounts for about 40%. Based on the simulation of element and isotope geochemical characteristics, Zhou et al. (1988) also found that the material contribution rate of mantle was over 60%, which was basically consistent with the research results of Lin et al. (2017). The upper part of the heat source is the heat reservoir dominated by highly radioactive granite, which is one of the main sources of heat in the lithosphere. Most of the southeastern coastal areas have the background of high heat generation (Wang et al. 2007), exceeding 2.8 μW/m^3. According to the temperature data of the existing boreholes in the southeast coastal area, the geothermal gradient in the southeast coastal area is 20–40℃/km. The temperature of the hot reservoir at the depth of 5km may reach 180℃ (Li et al. 2020). Combined with gravity and wide-field electromagnetic characteristics, the thermal reservoirs in the study area may be granodiorite and monzogranite, which covers the whole area within a wide range of depth.

Several large fault zones are exposed in the southeast coastal area, such as Changle-Shaoan, Nanxi-Lufeng, Zhenghe-Dapu and Shaowu-Heyuan fault zones (Fig. 1). These large faults transfer the deep heat to the shallow zones and hot springs frequently occur at the intersections of large faults with the shallow tensile faults (Teng et al. 2017). Although the occurrence of hot spring may not be directly related to the regional main fault, it is closely related to the secondary fault (Li et al. 2020). The hot springs in Zhangzhou Basin of Fujian Province are mainly arranged in the northeast direction, which reflects that the heat source of underground hot water is mainly controlled by the northeast direction structure (Nian, 2008). For the location of individual hot spring, most of them are located at the intersection of the NE- and NW- trending faults. The NW-trending faults are the newest structures in the region, with good transmissivity and storativity, which can provide the main recharge source and runoff channel for geothermal water (Pang, 1987). According to the results of structural interpretation, the NW-trending faults F12 and HT-F1 are the main hydraulic controlling structures, and the NE-trending faults F33 and F2 are the main thermal controlling structures.

Meteoric precipitation can infiltrate to and cool geothermal reservoir, but heat retaining cover with low thermal conductivity can reduce the effect. This cover layer is usually composed of sedimentary rock or volcanic rock, and sometimes it can also be weathered layer with appropriate thickness (Li et al. 2020). The thickness of the cover layer and the development of faults play an important role in heat preservation (He et al. 2020). There is a direct relationship between the sag and the cover layer in the study area. Sags generally refer to areas with deep quaternary and weathered fracture zones, and the deepest can reach 300 m.

Through the above analysis of the geothermal systems, the geothermal resources of medium-low temperature in Hongtang Area of Xiamen should be convective geothermal resources, mainly controlled by regional deep faults. The geothermal system should meet four conditions: Heat source, geothermal reservoir, heat conductive fault and heat retaining cover (Wang et al. 2016; Lu et al. 2017; Shi et al. 2019; Liu et al. 2020), which is a quaternary heat accumulation model. According to these conditions, the author proposed the genetic conceptual model of the hydrothermal systems of medium-low temperature in this area (Fig. 6).

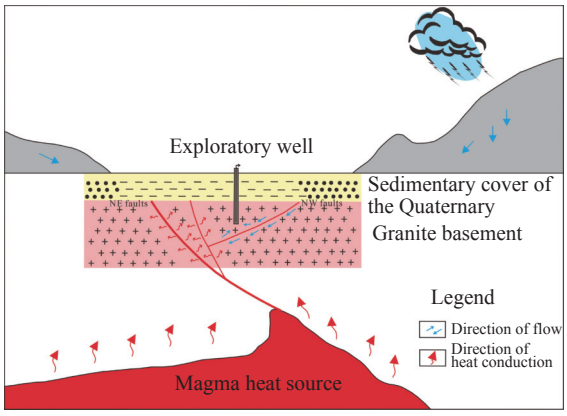

Fig. 6 Conceptual model of the ternary heat accumulation in Hongtang Area of Xiamen (Modified from Li TX et al. (2020))

5.3 Target areas of geothermal exploration and inspection

According to the heat accumulation model in this area, the delineation of geothermal exploration target area should meet four conditions: Heat source, geothermal reservoir, heat conductive fault and heat retaining cover. The deep rock mass in Hongtang area of Xiamen is granite and granodiorite. The heat source and geothermal reservoir in the area are consistent with the regional geothermal conditions. Therefore, more attention should be paid to fault and cover conditions in the delineation of geothermal exploration targets. The NE trending F12 and HT-F1 faults in the area are regional faults with compression-shear characteristics, which can transfer deep thermal energy to shallow rock mass. The EW trending F33, F2 faults and other NW trending secondary faults have tension-shear characteristics, good for groundwater circulation. These faults act as hydraulic conductive structures to extract thermal energy from the rock mass via groundwater transportation. Therefore, the intersection of compression-shear and tension-shear faults often has good geothermal conditions. In addition, the interpretation results show that there are small sags in the area, characterized by shallow coverage, small scale, but well-shaped. These local sags can be used as heat retaining cover and play an important role in geothermal preservation. The sags in the area mostly occur in the fault zones and have good water yield property, which are sustainable exchange zone of deep geothermal energy. After comprehensive analysis, the sags at the intersection of main faults F12, HT-F1 and F33 are found to be large and deep, classified as the primary target area of geothermal exploration (Fig. 5B). The NW-, EW- and NE-trending secondary faults are interconnected with the primary faults at depth in the area. The intersection of the faults (F12 and HT-F6; F12 and HT-F2; HT-F9, HT-F10 and F12; F12 and HT-F11; F33 and HT-F3; HT-F8 and HT-F3; HT-F2, HT-F10 and HT-F1) can be delineated as the secondary target area of geothermal exploration (Fig. 5B).

In this study, gravity and wide-field electromagnetic methods were used to investigate gravity anomalies and electromagnetic characteristics in the study area, on the basis of which, the distribution of faults and sags were interpreted and the geothermal exploration target areas were delineated. However, there are uncertainties in the survey and interpretation during the research process. In order to test the reliability of the results, a geothermal hole (Dr01, with footage of 603.31m) was drilled at 100 meters from the direction of No. 40, Xinxue Village, Hongyong Town, Xiamen City, Fujian Province (Fig. 6B). DR01 is located at the intersection of primary fault F33 and HT-F1, which has better conditions regarding faults and sedimentary cover. The temperature measurement curve of Dr01 shows that the water temperature rises to 36℃ at the depth of 0–500 m and then tends to be stable after 500 m (Fig. 7), indicating that the Hongtang area of Xiamen is a convective geothermal system. The geothermal resources are mainly transferred from deep thermal energy to shallow rock mass by regional faults, while geothermal gradient is a relatively weak factor, which explains that the temperature curve tends to be stable after reaching a certain depth. In the meantime, the temperature curve of Dr01 also proves that the heat accumulation model of Hongtang in Xiamen conforms to the geothermal geological characteristics of this area, and the interpretated structures and depressions in this area have high reliability, which can provide strong support for the subsequent development and utilization of geothermal resources.

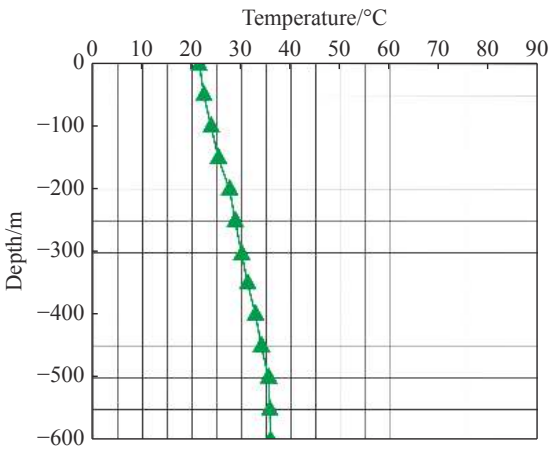

Fig. 7 Temperature curve of drilling Dr01 in Hongtang area of Xiamen

6 Conclusions

The convective geothermal system in Hongtang Area of Xiamen should have four conditions: Heat source, geothermal reservoir, heat conductivity fault and heat retaining cover, which form a quaternary heat accumulation model. Based on the interpretation of gravity anomaly in Hongtang area of Xiamen, the NW trending primary faults F12 and HT-F1, NE trending primary faults F33 and F2, and 10 secondary faults were identified. The sags are distributed along the inferred faults. The sags at the intersection of main faults F12, HT-F1and F33 are large and deep, which are delineated as the

primary target area of geothermal exploration. The intersection of faults (F12 and HT-F6; F12 and HT-F2; HT-F9, HT-F10 and F12; F12 and HT-F11; F33 and HT-F3; HT-F8 and HT-F3; HT-F2, HT-F10 and HT-F1) can be delineated as the secondary target area of geothermal exploration. The temperature curve of Dr01 shows that the temperature stays at 36℃ below the depth of 500 m. The results confirm that the heat accumulation model, the inferred faults and sags in Hongtang Area of Xiamen have high reliability, which can provide strong support for the subsequent development and utilization of geothermal resources.

Acknowledgements

This research was supported by the National Natural Science Foundation of China (Grants Nos. 41902242) and the Geological Survey Projects Foundation of the Institute of Hydrogeology and Environmental Geology (Grants Nos. DD20190303, DD20221773).

References

Chen PR, Hua RM, Zhang BT, et al. 2002. Early Yanshanian post-orogenic granitoids in the Nanling region: Petrological constraints and geodynamic settings. Science in China Series D: Earth Sciences, 45(8): 755-768.

Chen ZJ, Kong XR, Zhou WH, et al. 1992. Geothermal and geophysical research in Fujian province. Beijing: Science and Technology Press of China: 1-273. (in Chinese)

Fang SM, Zhang XK, Jia SX, et al. 2002. Muhis-scale decomposition of Bouguer gravity anomaly and seismic activity in North China. Journal of Geodesy and Geodynamics, 22(1): 34-39. (in Chinese)

Gao J, Zhang HJ, Zhang SQ, et al. 2018. Three-dimensional Magnetotelluric imaging of the geothermal system beneath the Gonghe Basin, northeast Tibetan plateau. Geothermics, 76: 15-25.

Goldstein MA, Strangway DW. 1975. Audio-frequency magnetotellurics with a grounded electric dipole source. Geophysics, 40(4): 669-683.

Hao TY, Liu YK, Duan C. 1997. The characteristic of geophysical field in the East China and adjacent regions and its tectonics significance. Acta Geophysica Sinica, 40(5): 677-690. (in Chinese)

He JS. 2019. Theory and technology of wide field electromagnetic method. The Chinese Journal of Nonferrous Metals, 29(9): 1809-1816. (in Chinese)

He JS. 2020. New research progress in theory and application of wide field electromagnetic method. Geoohysical & Geochemical Exploration, 44(5): 985-990. (in Chinese)

He ZL, Zhang Y, Feng JY, et al. 2020. Classification of geothermal resources based on engineering considerations and HDR EGS site screening in China. Earth Science Frontiers, 27(1): 081-093. (in Chinese)

Li P, Cai HT, Jin X, et al. 2019. Basement structure beneath the southeastern margin in Chinese continent. Chinese Journal of Geophysics, 62(8): 2991-3003. (in Chinese)

Li TX, Lin WJ, Gan HN, et al. 2020. Research on the genetic model and exploration progress of hot dry rock resources on the southeast coast of China. Journal of Geomechanics, 26(2): 187-200. (in Chinese)

Liao ZJ. 2012. Deep-circulation hydrothermal systems without magmatic heat source in Fujian province. Geoscience, 26(1): 85-98. (in Chinese)

Lin WJ, Wang FY, Gan HN, et al. 2015. Site selection and development prospect of a hot dry rock resource project in Zhangzhou geothermal field, Fujian province. Science & Technology Review, 33(19): 28-34. (in Chinese)

Lin WJ, Gan HN, Wang GL, et al. 2016. Occurrence prospect of HDR and target site selection study in Southeastern of China. Acta Geologica Sinica, 90(8): 2043-2058. (in Chinese)

Lin WJ, Gan HN, Wang GL. 2019. Geothermal resources survey of Xiamen-Qiongbei region of southeast China continent. Beijing: China Geological Survey. (in Chinese)

Lin LF, Sun ZX, Wang AD, et al. 2017. Radioactive geochemical characteristics of Mesozoic granites from Nanling region and southeast coastal region and their constraints on lithospheric thermal structure. Acta Petrologica Et Mineralogica, 36(4): 488-500. (in Chinese)

Liu F, Wang GL, Zhang W, et al. 2020. Using TOUGH2 numerical simulation to analyse the geothermal formation in Guide basin, China.

Journal of Groundwater Science and Engineering, 8(4): 328-337.

Lu C, Lin WJ, Gan HN, et al. 2017. Occurrence types and genesis models of hot dry rock resources in China. Environmental Earth Sciences, 76(19): 646.

Ma ZJ, Gao XL, Song ZF. 2006. Analysis and tectonic interpretation to the horizontal-gradient map calculated fromBouguer gravity data in the China mainland. Chinese Journal of Geophysics, 49(1): 106-114. (in Chinese)

Nian WZ. 2008. Formation model of geothermal field and its relation with control structure in Zhangzhou. Safety and Environmental Engineering, 15(4): 30-33. (in Chinese)

Pang ZH. 1987. Zhangzhou basin geothermal system-Genesis model, energy potential and the occurrence of thermal water. Beijing: Institute of Geology and Geophysics: CAS. (in Chinese)

Shao PA. 2013. Analysis on relationship between 1: 200 000 residual gravity anomaly of the Henan Province and the elements of geotectonic. Earth Science and Technology, (9-10): 96-10. (in Chinese)

Shi M, Kang FX, Zhang J, et al. 2019. Occurrence mechanism and geothermal exploration model of low-medium temperature geothermal systems of convective type in Jiaodong Peninsula. Geological Review, 65(5): 1276-1287. (in Chinese)

Teng JW, Si X, Zhuang QX, et al. 2017. Abnormal structure of crust and mantle and analysis of deep thermal potential in Fujian continental margin. Science Technology and Engineering, 17(17): 6-38. (in Chinese)

Wan TF, Chu MJ. 1987. Listric active fault of Fujian and Taiwan. Earth Science-Journal of Wuhan College of Geology, 12(1): 2l-29. (in Chinese)

Wan TF, Chu MJ, Chen MY. 1988. Thermal regimes of the lithophere and geothermal resources potential in Fujian Province. Acta Geologica Sinica, 62(2): 178-189. (in Chinese)

Wang GL, Lin WJ, Zhang W, et al. 2016. Research on formation mechanisms of hot dry rock resources in China. Acta Geologica Sinica (English Edition), 90(4): 1418-1433.

Wang GL, Wang WL, Zhang W, et al. 2020. The status quo and prospect of geothermal resources exploration and development in Beijing-Tianjin-Hebei region in China. China Geology, 3: 173-181.

Wang YJ, Fan WM, Sun M, et al. 2007. Geochronological, geochemical and geothermal constraints on petrogenesis of the Indosinian peraluminous granites in the South China Block: A case study in the Hunan Province. Lithos, 96(3-4): 475-502.

Ward SH. 1980. Electrical, electromagnetic and magnetotelluric methods. Geophysics, 45(11): 1659-1666.

Wu CF. 2019. Magnetotelluric Imaging of the Zhangzhou Basin Geothermal Zone, Southeastern China. China University of Geosciences: Doctoral Dissertation. (in Chinese)

Xiong SB, Jin DM, Sun KZ, et al. 1991. Some characteristics of deep structure of the Zhangzhou geothermal field and it's neighbourhood in the Fujian Province. Chinese Journal of Geophysics, 34(1): 55-63. (in Chinese)

Zhang BJ, Zhao T, Li YY, et al. 2019. The hydrochemical characteristics and its significance of geothermal water in both sides of large fault: Taking northern section of the Liaokao fault in north China as an example. China Geology, 2: 512-521.

Zheng HW, Gao R, Li TD, et al. 2013. Collisional tectonics between the Eurasian and Philippine sea plates from tomography evidences in southeast China. Tectonophysics, 606: 14-23.

Zhuang QX. 2015. Geothermal resources exploration in Fujian province. Energy and Environment, (1): 1-4. (in Chinese)

Zhou XM, Li WX. 2000. Origin of Late Mesozoic igneous rocks in southeastern China: Implications for lithosphere subduction and underplating of mafic magmas. Tectonophysics, 326(3-4): 269-287.

Zhou XR, Chen AG, Song XH, et al. 1988. Research on the genesis and Rb-Sr isotope age of granitic intrusion of Zhangzhou, Fujian, China. Bulletin of Nanjing Institute of Geological Mineral and Resources, (2): 58-70. (in Chinese)